JOURNAL OF KUFA–PHYSICS
journal.uokufa.edu.iq/index.php/jkp/index | ISSN: 2077–5830

Phase-Matching Optimization and Walk-off Analysis in LBO Crystals

Ruqayah Majid Hilal[1], Sundus Y. Hasan[2]

[1]*Physics Department, Education College for Girls, Kufa University*

[*]*Corresponding Author E-mail:* ruqayyahm.alhasnawi@student.uokufa.edu.iq
sundus.alasadi@uokufa.edu.iq

ARTICLE INF.

Article history:
Received: 15 APR., 2026
Revised: 17 MAY., 2026
Accepted: 09 JUN., 2026
Available Online: 28 JUN. 2026

Keywords:

LBO crystal,
SHG,
phase matching,
walk-off,
Fresnel equation,
Sellmeier equation.

ABSTRACT

Lithium Triborate (LBO) is a biaxial nonlinear optical crystal widely used for laser frequency conversion owing to its broad transparency range (160–2600 nm), high damage threshold, and favorable phase-matching properties. This study presents a comprehensive numerical model based on solving the Fresnel equation with modified Sellmeier coefficients to analyze spectral birefringence, critical phase-matching angles, walk-off, and OPO tuning in LBO. For Type-I SHG at 1.064 μm, phase matching is achieved in the XY plane at $\varphi = 16.13°$ ($\Delta n = 2.85\times10^{-6}$) and in the XZ plane at $\theta = 30.99°$ ($\Delta n = 2.34\times10^{-5}$), with a global off-axis optimum at $\theta = 67.42°$, $\varphi = 25.59°$ ($\Delta n = 1.02\times10^{-7}$). For Type-II SHG, the XY plane yields phase matching at $\varphi = 51.35°$ ($\Delta n = 9.06\times10^{-6}$), with an off-axis optimum at $\theta = 39.43°$, $\varphi = 64.41°$ ($\Delta n = 6.15\times10^{-8}$). Phase matching is not achievable in the YZ plane for either type. Walk-off peaks at ~0.95° near 0.8 μm in the XY plane and ~1.38° at 1.1 μm in the XZ plane. OPO tuning pumped at 532 nm demonstrates broad coverage, with Type-II extending the signal to 2.5 μm via azimuthal rotation in the XY plane.

DOI: https://doi.org/10.31257/2018/JKP/2026/v18.i1.23796

تحسين مطابقة الطور وتحليل الانحراف في بلورات LBO

رقيه ماجد هلال[1] ، سندس ياسين حسن[2]

قسم الفيزياء كلية التربية للبنات جامعة الكوفة

الكلمات المفتاحية:

بلورة LBO،
SHG،
تطابق الطور
، الانزياح،

الـــخُـــلاصـــة

تعد بلورة ثلاثي بورات الليثيوم (LBO) بلورة بصرية غير خطية ثنائية المحور تستخدم على نطاق واسع لتحويل تردد الليزر نظرا لنطاق شفافيتها الواسع (160-2600) نانومتر وعتبة الضرر العالية وخصائص تطابق الطور. تقدم هذه الدراسة نموذجا عدديا شاملا يعتمد على حل معادلة فرينل مع معاملات سيلمير المعدلة لتحليل الانكسار المزدوج الطيفي وزوايا تطابق الطور الحرجة

والانزياح وتوليف OPO في LBO بالنسبة SHG من النوع الأول عند 1.064 مايكرومتر تم تحقيق تطابق الطور في المستوي XY عند φ = 16.13º وفي مستوي XZ عند θ = 30.99º ($\Delta n=2.34*10^{-5}$) مع وجود نقطة مثالية خارج المحور عند الزوايا θ=67.42º وφ=25.59º ($\Delta n=1.02*10^{-7}$) اما SHG من النوع الثاني فان المستوي XY يحقق مطابقة الطور عند الزاوية φ=51.35º ($\Delta n=9.06*10^{-6}$) مع نقطة مثالية خارج المحور عند θ=39.43º وφ=65.41º ($\Delta n=6.15*10^{-8}$). ولا يمكن تحقيق مطابقة الطور في المستوي YZ لكلا النوعين. يصل الانحراف الزاوي الى ذروته عند حوالي 0.95º بالقرب من الطول الموجي 0.8µm في المستوي XY وحوالي 1.38º عند 1.1µm في المستوي XZ ويظهر ضبط المذبذب البصري البارامتري عند ضخه بشعاع ليزر طولة الموجي 532nm تغطية واسعة النطاق، حيث يمتد الطول الموجي لإشارة المخرج من النوع الثاني ليصل الى 2.5µm عبر التدوير السمتي في المستوي XY .

معادلة فرينيل،
معادلة سليمير

1. INTRODUCTION

Lithium Triborate (LiB_3O_5, LBO) is one of the most important nonlinear optical crystals in modern photonics, that are widely employed for laser frequency conversion due to its exceptional combination of properties: A broad transparency range spanning between 160–2600 nm, a high laser damage threshold, moderate nonlinear coefficients, and a relatively small spatial walk-off angle compared to other birefringent materials such as KTP and BBO [1, 2]. These characteristics make LBO particularly suitable for high-power second-harmonic generation (SHG), optical parametric oscillation (OPO), and sum-frequency generation (SFG) across the ultraviolet, visible, and near-infrared spectral regions [1, 2, 3].

A further practical advantage of LBO is its ability to support both critical phase matching (CPM), achieved through angular orientation of the crystal, and non-critical phase matching (NCPM), achieved through temperature tuning along a principal crystallographic axis. In NCPM, the walk-off angle vanishes identically, for example, SHG of 1.0642 mm radiation achieves NCPM at approximately 148C^o along the X axis[4, 5], allowing the use of longer crystal lengths without spatial beam distortion and yielding higher conversion efficiencies, a property that has made LBO the preferred choice for high-power continuous-wave and pulsed frequency conversion systems

Unlike uniaxial crystals such as the KDP or BBO, LBO belongs to the orthorhombic crystal system and is a biaxial anisotropic medium, that is characterized by three distinct principal refractive indices $n_x < n_y < n_z$. In such a medium, the refractive index that is experienced by a propagating wave depends strongly on both the wavelength and the full propagation direction, specified by the polar angle θ and azimuthal angle φ. Wave propagation must therefore be described using the complete tensorial dielectric formalism, in which the two allowed refractive indices for any given propagation direction are obtained by solving the Fresnel equation derived

from Maxwell's equations [6]. The directional dependence of these effective refractive indices is fundamental to determining the birefringence behavior and the phase-matching conditions available in the crystal.

Efficient nonlinear frequency conversion requires satisfaction of the phase-matching condition $\Delta k = 0$, which ensures phase coherence between the nonlinear polarization wave and generated wave throughout the interaction length, as described by the coupled wave equations [7, 8]. In birefringent phase matching, the angular dependence of the refractive indices is exploited to compensate for material dispersion. In biaxial crystals like LBO, this process is inherently more complex than in uniaxial crystals due to the presence of two optical axes and fully direction-dependent polarization eigenmodes, requiring a two-angle description of the propagation geometry.

Since the original discovery and characterization of LBO by Chen et al. [3], considerable effort has been devoted to determining its Sellmeier equations [13], phase-matching angles for SHG [10], OPO tuning characteristics [11], and laser damage properties [12]. However, the majority of existing studies treat phase matching within individual principal planes (XY, XZ, or YZ) and address walk-off, angular optimization, and parametric tuning as separate analyses. A unified electromagnetic framework that simultaneously connects Fresnel-based wave propagation with full two-dimensional angular phase-matching optimization, walk-off quantification, and OPO parametric tuning curves, within a single self-consistent numerical model, has not been reported for LBO.

In the present work, we develop and presents such a comprehensive numerical model. Effective refractive indices are obtained by solving the Fresnel equations in the anisotropic medium using modified Sellmeier coefficients for all three principal axes. Moreover, Spectral birefringence is characterized across all principal planes. Phase-matching conditions for Type-I and Type-II SHG at a fundamental wavelength of 1.064 μm are determined not only within the three principal planes but also through full two-dimensional angular scans (θ, φ) to identify global optimal cut angles. The spatial walk-off angle is quantified as a function of both wavelength and propagation direction. Finally, the angular tuning characteristics of an OPO pumped at 532 nm are analyzed for both Type-I and Type-II interactions. The results provide practical and systematic guidelines for the design and optimization of LBO-based nonlinear optical devices.

2. Theoretical framework and numerical method

The refractive index (and various optical properties) of Lithium Triborate, LBO, were investigated in previous work using modified Sellmeier equation (eq.1) [13].

$$n^2(\lambda) = A + \frac{B\lambda^2}{\lambda^2 - C} + \frac{D\lambda^2}{\lambda^2 - E} + F\lambda^2 \quad (1).$$

where λ is the vacuum wavelength in micrometers and the six fitting parameters A through F are specific to each polarization axis. The numerically fitted values adopted in this work are collected in Table 1.

Table 1. Values of the six parameters of the modified Sellmeier eq.1 for the refractive index of the three components of the LBO.

	A	B	C (μm²)	D	E (μm²)	F (μm⁻²)
n_x	0	1.2366	0.0056	1.209	0.0056	−0.0074
n_y	0	1.2568	0.0053	1.2837	0.0053	−0.0206
n_z	0	1.2742	0.0059	1.3049	0.0059	−0.0145

In this study, (Eq.1) is utilized to analyze the spectral birefringence behavior, phase matching cut angles, and walk-off angles. The following sections detail these parameters.

2.1 Spectral Birefringence Behavior

The LBO is a biaxial crystal belonging to the orthorhombic system, which is characterized by three principal refractive indices: n_x, n_y, and n_z. For light propagating in an arbitrary direction defined by the unit wave normal vector $\hat{k}$ = (s_x= sin(□)cos(φ), s_y= sin(□)sin(φ), s_z=cos(□)), the two allowed refractive indices, n_1 and n_2, are computed from the Fresnel equation in its quadratic form. Mathematical Derivation of the Fresnel Equation To rigorously derive this relation, we begin with Maxwell's curl equations in a charge-free, non-magnetic anisotropic medium [6]:

$$\nabla \times \boldsymbol{E} = -\mu_{\circ} \frac{\partial H}{\partial t} \quad (2)$$

$$\nabla \times \boldsymbol{H} = \varepsilon_{\circ} \varepsilon_r \frac{\partial E}{\partial t} \quad (3)$$

Where $\varepsilon_r = diag\,(n_x^2, n_y^2, n_z^2)$, is the principal relative permittivity tensor, **E** and **H** are the electric and magnetic fields vectors.

Assuming a monochromatic plane wave $\boldsymbol{E}(r,t) = \boldsymbol{E}_{\circ} e^{i(\boldsymbol{k}.\boldsymbol{r}-\omega t)}$, combining Maxwell's equation to eliminate H yields the vector wave equation:

$$(4)\ \boldsymbol{k} \times (\boldsymbol{k} \times \boldsymbol{E}) + \frac{\omega^2}{c^2}\, \varepsilon_r \,.\boldsymbol{E} = 0$$

Applying the vector identity

$k \times (k \times E) = \boldsymbol{k}(\boldsymbol{k}.\boldsymbol{E}) - k^2 \boldsymbol{E}$. and substituting the wave vector $\boldsymbol{k} = \frac{n\omega}{c}\boldsymbol{s}$ (where **s** is the unit propagation vector), we obtain the eigenvalue equation for the optical field:

$$(\varepsilon_r - n^2 I)E + n^2 s(s.E) = 0 \quad (5)$$

For non-trivial field solutions (**E**=0), the determinant of the system must vanish, leading to Fresnel's determinant equation:

$$det|\varepsilon_r - n^2(I - ss)| = 0 \quad (6)$$

Resolving this determinantal component along the principal axes yields the final characteristic Fresnel equation for the wave normal:

$$\frac{s_x^2}{n^2-n_x^2} + \frac{s_y^2}{n^2-n_y^2} + \frac{s_z^2}{n^2-n_z^2} = 0 \quad (7)$$

Solving this quadratic equation for n^2 yields two distinct roots, representing the indices of the two orthogonal polarization modes at a given wavelength and propagation angle.

$$An^4 + Bn^2 + C = 0 \quad (8)$$

$$n^2 = \frac{B \mp \sqrt{B^2-4AC}}{2A} \rightarrow n_{1,2} = \left(\frac{B \mp \sqrt{B^2-4AC}}{2A}\right)^{1/2} \quad (9)$$

Where A=1

$$B = -[s_x^2(n_y^2 + n_z^2) + s_y^2(n_x^2 + n_z^2) + s_z^2(n_x^2 + n_y^2)]$$

$$C = s_x^2 n_y^2 n_z^2 + s_y^2 n_x^2 n_z^2 + s_z^2 n_x^2 n_y^2$$

2.2 Optical Axes of the LBO

A biaxial crystal possesses two optical axes, directions of wave propagation along which the two allowed refractive indices become equal and the crystal behaves as if locally isotropic. These directions are also referred to as the bi-normal axes, corresponding to the circular cross-sections of the optical indicatrix. Along any other propagation direction, the two components travel with different phase velocities, giving rise to birefringence.

For the orthorhombic biaxial crystal-like LBO satisfying $n_x < n_y < n_z$, both optical axes lie within the XZ principal plane ($\varphi = 0°$), symmetrically positioned at angles $+V_z$ and $-V_z$ from the Z-axis. The total angular separation between them is therefore $2V_z$. The angle V_z is determined by the three principal refractive indices through the relation [1, 6]:

$$\tan(V_z) = \frac{n_z}{n_x}\sqrt{\frac{n_y^2-n_x^2}{n_z^2-n_y^2}} \quad (10)$$

This expression is derived directly from the condition that the two roots of the Fresnel equation (Eq. 7) become degenerate, $n_1 = n_2$, which is satisfied precisely when the wave normal points along an optical axis direction. Since n components are all wavelength-dependent through the Sellmeier equation, V_z is also dispersive and shifts with wavelength across the transparency range of the crystal.

It is important to distinguish the optical axes from the principal crystallographic axes X, Y, Z. The Walk-off vanishes along the principal axes, not along the optical axes. Propagation in the immediate vicinity of an optical axis gives rise to the phenomenon of internal conical refraction [3], which should be avoided in practical nonlinear device design by selecting phase-matching angles sufficiently removed from V_z.

The numerical computation proceeds in the following steps: (1) the Sellmeier coefficients (Table 1) are used to evaluate $n_x(\lambda)$, $n_y(\lambda)$, $n_z(\lambda)$ on a dense wavelength grid spanning 0.25-2.5μm (2) for each propagation direction (θ, φ) on an angular grid of 0.1º resolution, the Fresnel equation (Eq. 7) is solved analytically via (Eq. 9) to obtain the two eigenmode indices n_1 and n_2, phase-matching conditions are identified where the mismatch $\Delta n = | n_2(2\omega) - n_1(\omega) |$ falls below a threshold of 10^{-4}, (3) the walk-off angle is computed form Eq. (14) using central difference numerical differentiation, and OPO tuning curves are generated by enforcing energy conservation ωp =ωs +ωi simultaneously with the phase-matching condition for each crystal orientation All calculations were performed in MATLAB version 2015.

3. Results and discussion

3.1 Optical axes of the LBO

The optical axis angle V_z was computed in Eq. 10) using the modified Sellmeier coefficients of Table 1. As shown in Fig. 1, V_z has been exhibits a non-monotonic spectral dependence. Increasing from ~49° at short wavelengths (λ ≈ 0.25 μm) to a maximum of ~55° in the visible (λ ≈ 0.62 μm), then decreasing slightly to 52.9° at λ = 1.1 μm. This behavior reflects the unequal dispersion of the three principal indices. Values at λ = 0.532 μm and λ = 1.064 μm (Table 2) fall within this range and agree well with the literature range of ~51°–55° reported in [1, 3]. The total angular separation 2Vz is reported in Table 2 to confirm that all selected phase-matching cut angles are sufficiently removed from the optical axis directions, thereby avoiding internal conical refraction.

Table 2. Principal refractive indices of LBO and optical axis angles V_z calculated from the modified Sellmeier equation at λ=1.064μm and λ=0.532μm

λ(μm)	n_x	n_y	n_z	Vz (°)	2Vz (°)
0.532	1.578883	1.607219	1.621698	±54.98	109.97
1.064	1.565050	1.590323	1.605053	±53.16	106.33

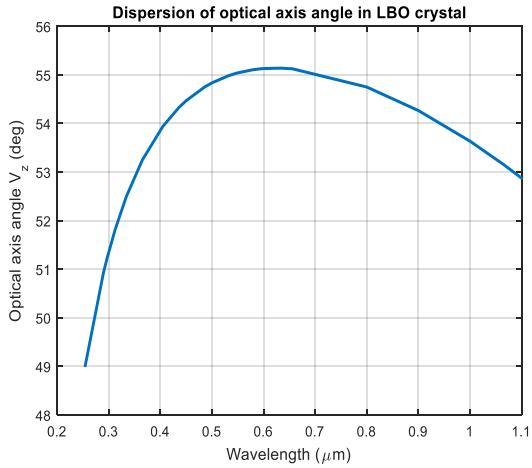

Fig. 1: The spectral Dependence of the Optical Axis Angle V_z in LBO Crystal

The total angular separation $2V_z$ is reported to aid verification that all selected phase-matching cut angles are sufficiently removed from the optical axis directions, thereby avoiding internal conical refraction.

3.2 Spectral Birefringence Behavior

The spectral birefringence $\Delta n = |n_2 - n_1|$ has been evaluated using (Eq.7) with the Sellmeier coefficients of Table 1, across the principal planes of the LBO from 0.25 to 1.1 μm. Results are shown in Fig. 2.

a) XZ Principal Plane (φ = 0°, varying θ) Birefringence shows strong angle-dependence governed by proximity to the optical axis V_z. At θ = 30°, Δn peaks near ~0.0175 at λ ≈ 0.52 μm, remaining large throughout. At θ = 60°, a characteristic trough appears near λ ≈ 0.65 μm (Δn ≈ 0.0037), where V_z reaches its closest approach to this propagation direction and the two eigenmodes nearly equalize. At θ = 75° and 90°, curves decrease monotonically from UV toward a minimum near 0.70 μm.

b) YZ Principal Plane (φ = 90°, varying θ) All curves show birefringence uniformly in the range ~0.03–0.05, decreasing smoothly toward longer wavelengths. No near-zero birefringence occurs here because both optical axes of LBO lie exclusively within the XZ plane, so the condition $n_1 = n_2$ is never satisfied in the YZ plane.

c) Along the Z-axis (θ = 0°, varying φ) Birefringence is independent of φ, measuring $\Delta n = |n_x - n_y|$, the smallest component of the LBO. A broad peak appears near λ = 0.4–0.5 μm. Walk-off vanishes identically in this configuration.

d) XY Plane (θ = 90°, varying φ) One eigenmode always carries n_z; the other varies continuously between n_x and n_y with azimuthal angle. This produces the widest spread of Δn values across all panels, explaining why the XY plane offers the greatest birefringence tunability and yields the most favorable phase- matching geometry for both Type-I and Type-II SHG.

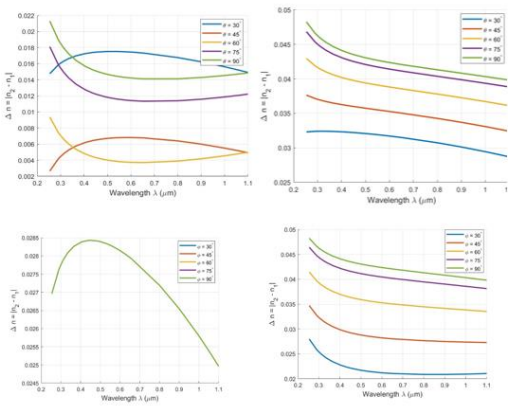

Fig. 2: Birefringence $\Delta n=n_2-n_1$ as a function of wavelength for LBO, at different propagation angles. Top left figure: φ = 0, θ = 30, 45, 60, 75, and 90, XZ-plane. Top right figure: φ = 90, θ = 30, 45, 60, 75, and 90, YZ plane. Bottom left figure: θ = 0, φ = 30, 45, 60, 75, and 90. Bottom right figure: θ = 90, φ = 30, 45, 60, 75, and 90, XY plane.

3.3 Phase-Matching Cut Angles

3.3.1 Type-I Phase Matching (SHG - 1064nm)

Phase-matching conditions for Type-I SHG at 1.064 μm have been determined by solving Eq. 7) within each of the three principal planes and via a full two-dimensional angular scan, as detailed below.

3.3.1.1 Angular Phase Matching in the Principal Planes of LBO

Angular phase matching, which is referred to as critical phase matching (CPM),is achieved by orienting the crystal such that the propagation direction (θ, φ) satisfies the phase-matching condition for the interacting waves [1, 2]. While LBO also supports non-critical phase matching (NCPM) through temperature tuning along a principal crystallographic axis, where walk-off vanishes identically, the present study focuses exclusively on angular CPM, which provides room-temperature operation and broad wavelength coverage through crystal orientation.

For a biaxial crystal such as the LBO, the phase-matching directions are most conveniently found by restricting propagation to one of the three principal planes, XY, XZ, or YZ. This restriction is physically advantageous because within a principal plane one of the two allowed eigenmodes always carries a refractive index equal to a pure principal index, which simplifies both the Fresnel equation solution and the evaluation of the effective nonlinear coefficient. Outside the principal planes, both eigenmodes are mixed polarization states and the full two-dimensional angular analysis is required.

Within each principal plane, one of the two angles θ or φ is fixed by the plane geometry and the other serves as the single tuning parameter. Each principal plane offers a distinct phase-matching geometry, as follows:

a) Phase Matching in the XY-Plane (θ=90°)

In the XY-plane, propagation is perpendicular to the Z-axi s, so θ is fixed at 90° and the azimuthal angle φ is the only tuning parameter.

Using the Sellmeier equation (eq. 1), a numerical solution yields phase matching at 1064 nm for:

φ=16.13° (as shown in Fig.3-left) where the corresponding refractive indices:
$n_{slow}(\omega)=n_z(\lambda=1.064\mu m)=1.605053$,,
and $n_{fast}(2\omega)$ =1.605050 which calculated by solving eq.7, and
$\Delta n= \left|n_{fast}(2\omega) - n_{slow}(\omega)\right|=$
2.85×10^{-6}, where one mode always equals n_z exactly, giving maximum birefringence leverage.

The residual mismatch $\Delta n\sim10^{-6}$ confirms that near-perfect Type-I phase matching is achieved at this angle.

b) Phase Matching in the XZ-Plane (φ=0°)

In the XZ -plane, the azimuthal angle is fixed at φ=0° and θ serves as the tuning parameter. Matching occurred at θ = 30.99° (see Fig.3-right) with $\Delta n = 2.34*10^{-5}$. Although slightly larger than in the XY the mismatch remains sufficiently small for efficient SHG.

The V-shaped curve reflects the anisotropic nature of the crystal where $n_{slow}(\omega) = n_y(1.064\square m)$, and the other index $n_{fast}(2\omega)$ depends on the propagation direction within the optical indicatrix, which varies between nx and nz as θ changes from 0° to 90°. As the angle θ increases the birefringence decreases reaching a minimum near θ ≈ 31°, the phase matching cut angle,

where $n_{slow}(\omega) \approx n_{fast}(2\omega)$. Beyond this angle the refractive index difference increases again.

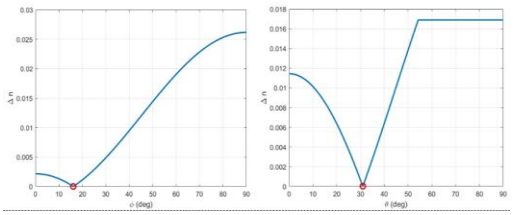

Fig. 3: Minimum effective refractive index difference (Δn) for Type I SHG phase matching in LBO at a fundamental wavelength of 1064 nm, as a function of (1) (left) azimuthal angle φ for propagation in the XY plane, and (2) (right) polar angle θ for propagation in the XZ plane. The red circles indicate the phase-matching cut angles at φ ≈ 16° (XY plane) and θ ≈ 31° (XZ plane), where Δn vanishes and the phase-matching condition $n_{slow}(\omega) = n_{fast}(2\omega)$ is satisfied.

c) Phase Matching in the YZ-Plane (φ=90°)

In the YZ -plane, φ is fixed at 90°and θ is the tuning parameter. There is no true phase matching that has been observed in the YZ plane. The minimum mismatch obtained was Δn = $1.38*10^{-2}$, which is too large to satisfy **Δk** = 0. This plane is generally less favored for the SHG of 1064 nm as the phase-matching angle may fall outside the practical angular range, The actual reason is that **in the YZ plane, no optical axis of the LBO is found** (both optical axes lie in the XZ plane), so the birefringence $\Delta n = |n_z - n_y|$ is always finite and positive but never large enough to compensate the dispersion between ω and 2ω at 1064 nm.

3.3.1.2 Phase-Matching Surface for Type-I SHG

To extend the analysis beyond the principal planes, a full two-dimensional angular scan has been performed through by simultaneously varying the polar angle θ and the azimuthal angle φ both over [0°, 90°] across the entire accessible orientation space of the LBO crystal. Fig.4 shows the phase-matching surface for Type-I Second Harmonic Generation (SHG). The surface illustrates the variation of the mismatch parameter $n_{fast}(2\omega, \theta, \varphi) - n_{slow}(\omega, \theta, \varphi)$.

The smooth shape structure of the surface reflects the anisotropic dispersion of the refractive index in the crystal. Since both eigenmode indices rely the propagation direction through using the optical indicatrix, the effective refractive indices vary continuously and smoothly with θ and φ across the full angular space.

The "Valley" region (Dark Blue) represents the most important part of the graph. The global minimum of $\Delta n = 1.02\times10^{-7}$ is located at θ = 67.42° and φ = 25.59°, representing the optimal off-principal-plane cut for Type-I SHG at 1.064 μm. The near-zero residual mismatch at this point confirms the fact that essentially perfect phase matching is achieved, and these angles define the crystal orientation that maximizes second-harmonic conversion efficiency. Inspection of Fig. 4 asserts the consistency with the principal-plane results of Fig. 2, the cross-section at θ = 90° reproduces the XY-plane minimum at φ = 16.13°, and the cross-section at φ = 0° reproduces the XZ-plane minimum

at θ = 30.99°, validating the two-dimensional model against the one-dimensional principal-plane scans.

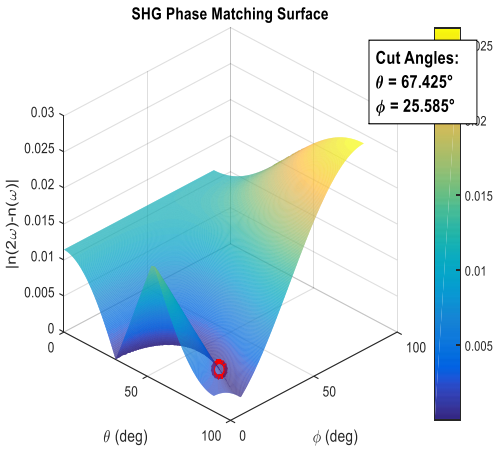

Fig.4: Phase-matching surface for Type-I second harmonic generation (SHG) at a fundamental wavelength of 1.064 μm, where the minimum mismatch occurs at θ=67.425° and φ=25.585°

To the best of the authors' knowledge, no published experimental measurements of off-principal-plane phase-matching angles in LBO are currently available for direct comparison. The present results therefore constitute theoretical predictions, whose consistency with the well-established principal-plane values provides confidence in the model's reliability.

Table. 3 shows a comparison of the three principal planes in addition to off principal for type I interaction for the LBO crystal.

plane	Phase-matching angle	$n_{slow}(\omega)$	$n_{fast}(2\omega)$	Δn
XY	φ=16.13, θ=90	1.605053	1.605050	$2.85*10^{-6}$
XZ	θ=0, ϕ=30.99	1.590323	1.590347	$2.34*10^{-5}$
YZ	φ=90, θ=3.24	1.565050	1.578883	$1.38*10^{-2}$
Off-axis	φ=25.5853°, θ=67.4247°	1.600824	1.600824	$1.013*10^{-7}$

3.4 Type-II Phase Matching (SHG at 1064nm)

In Type-II phase matching, the two lower-frequency waves have orthogonal polarizations. One lower-frequency wave is polarized along the "slow " axis, and the other is polarized along the "fast" axis. The higher-frequency wave is typically polarized along the fast axis. The condition must be satisfied is $n_{fast}(2\omega,\theta,\varphi) = (n_{slow}(\omega,\theta,\varphi) + n_{fast}(\omega,\theta,\varphi))/2$. i.e. the high-frequency wave's index must match the average of the slow and fast indices of the fundamental waves.

3.4.1 Angular Phase Matching in the Principal Planes of the LBO

a) Phase Matching in the XY-Plane (θ=90°)

Here Δn is defined as $|n_{fast}(2\omega, \varphi) - [n_{slow}(\omega, \varphi) + n_{fast}(\omega, \varphi)]/2|$, which must vanish for Type-II phase matching.

The left panel of Fig. 5 shows the variation of Δn as the azimuthal angle ϕ is varied from 0° to 90° with θ fixed at

90°, confining the propagation direction to the XY principal plane. The minimum value of Δn 9.06 $\times 10^{-6}$ (the red circle) is reached at φ=51.35° satisfying Δk ≈ 0**.** This identifies the "cut angle" in the XY plane which defines the required crystal orientation for Type-II SHG of 1.064 μm in the LBO at room temperature. At this angle, the three contributing indices are: $n_{fast}(2\omega)$ = 1.589996, $n_{fast}(\omega)$ = 1.574956, and $n_{slow}(\omega)$ = 1.605053, yielding an average fundamental index of $[n_{slow}(\omega) + n_{fast}(\omega)]/2$ = 1.590005, consistent with the near-zero residual mismatch.

Phase matching in the XY plane is favored because the large contrast between n_z (slow mode) and the azimuthally varying fast mode provides sufficient birefringence to bridge the averaged fundamental index condition required for Type-II interaction.

b) Phase Matching in the XZ-Plane (φ=0)

Type-II SHG in the XZ plane does not achieve phase matching; the minimum residual mismatch is Δn ≈ 1.2×10^{-3} occurs at θ = 0° corresponding to propagation along the Z-axis, but even at this angle the residual mismatch remains three orders of magnitude above the values achieved in the XY plane, which is too large to satisfy Δk = 0. This failure arises because in the XZ plane one fundamental eigen-mode always carries the fixed index $n_y(\omega)$, while the other varies between $n_x(\omega)$ and $n_z(\omega)$ as θ is tuned. The averaged fundamental index $[n_y(\omega) + n_{eff}(\omega)]/2$ required by the Type-II condition never reaches the second-harmonic index $n_{fast}(2\omega, \theta)$ at any angle θ, since the dispersion between ω and 2ω exceeds the birefringence range accessible within this plane. The non-zero mismatch throughout the entire angular range confirms that phase matching (Δk ≠ 0 for all θ) is unachievable in the XZ plane for Type-II SHG at 1.064 μm.

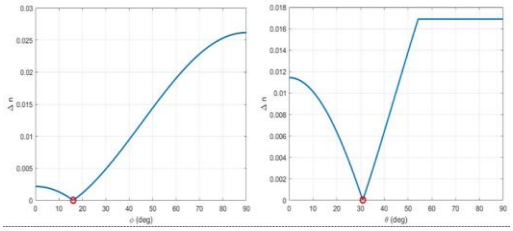

Fig. 5. Minimum effective refractive index difference (Δn) for Type II SHG phase matching in LBO at a fundamental wavelength of 1064 nm, as a function of (1) (left) azimuthal angle φ for propagation in the XY plane, The red circles indicate the phase-matching cut angles at φ ≈ 51 °and (2) (right) polar angle θ for propagation in the XZ plane, where no phase-matching condition is satisfied (minimum Δn ≈ 1.2×10^{-3}). the Type-II phase-matching condition $n_{fast}(2\omega) = [n_{slow}(\omega, \varphi) + n_{fast}(\omega, \varphi)]/2$ is satisfied.

c) Phase Matching in the YZ-Plane (φ=90)

Type-II SHG phase matching is not achievable in the YZ plane. The minimum residual mismatch of Δn ≈ 1.38×10^{-2} occurs at θ ≈ 11.44°, but this value is far from zero and therefore does not constitute true phase matching, since no propagation direction within this plane satisfies Δn=0.

This result is expected, as the YZ plane contains no optical axis of the LBO, the birefringence remains strictly finite throughout, and the additional averaging required by the Type-II condition further reduces the effective index contrast available for compensation.

Comparing the three principal planes, the XY plane yields the smallest mismatch ($\Delta n = 9.06\times10^{-6}$) and is the only plane where Type-II phase matching is achievable for 1.064 μm SHG in the LBO. The XZ and YZ planes exhibit residual mismatches approximately three and four orders of magnitude larger, respectively, confirming that Type-II interactions in LBO are geometrically constrained to the XY plane.

3.4.2 Phase-Matching Surface for Type-II SHG

To extend the Type-II phase-matching analysis beyond the principal planes, a full two-dimensional angular scan was performed by simultaneously varying θ and φ both over [0°, 90°]. The resulting phase-matching surface, plotted in Fig. 6, maps the Type-II mismatch parameter $\Delta n = |n_{fast}(2\omega) - [n_{slow}(\omega) + n_{fast}(\omega)]/2|$ as a function of both propagation angles.

Comparing the three principal planes, the XY plane yields the smallest mismatch ($\Delta n = 9.06\times10^{-6}$) and is the only plane where Type-II

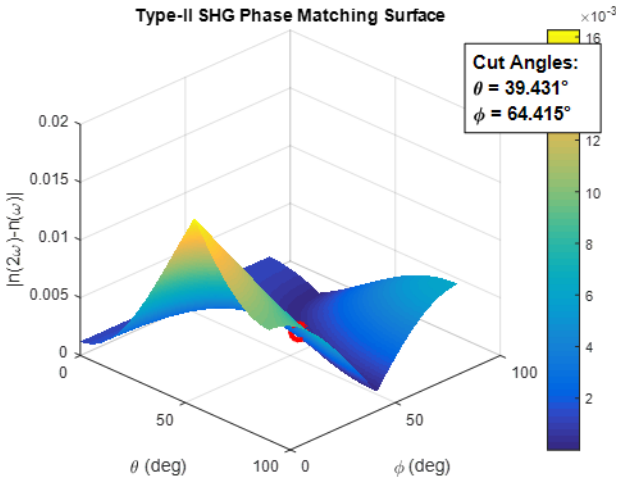

Fig.6: Phase-matching surface for Type-II second harmonic generation (SHG) at a fundamental wavelength of 1.064 μm, where the minimum mismatch occurs at φ=64.4147°, θ=39.4314°.

The surface rises steeply away from a narrow valley of near-zero mismatch, with the dark blue region identifying the locus of propagation directions closest to the Type-II phase-matching condition. Outside this valley, Δn increases rapidly, confirming that phase matching is highly sensitive to crystal orientation. The global minimum of $\Delta n = 6.15\times10^{-8}$ is located at θ = 39.43° and φ = 64.41°, identifying the optimal off-principal-plane cut angle for Type-II SHG at 1.064 μm. The residual mismatch of $\Delta n = 6.15\times10^{-8}$ at this optimal orientation confirms near-perfect Type-II phase matching, and is notably smaller than the Type-I off-axis optimum of $\Delta n = 1.02\times10^{-7}$ reported in section 3.3.1, indicating that the off-principal-plane geometry provides an

even tighter phase-matching condition for Type-II than for Type-I interactions.

This off-principal-plane optimum arises because neither the XZ nor the YZ plane alone provides sufficient birefringence contrast to satisfy the Type-II averaged condition, while a general (θ, φ) direction allows simultaneous access to all three principal index dispersions, providing the additional degree of freedom needed to satisfy the condition more precisely. The result also confirms that restricting the search to principal planes would miss the globally optimal crystal cut by approximately one order of magnitude in Δn.

The cross-section of the surface at θ =90° reproduces the XY-plane minimum at φ = 51.35° with Δn = 9.06×10^{-6}, and the cross-section at φ=0° confirms the absence of phase matching in the XZ plane, consistent with the principal-plane results of section 3.3.1.

Table 4: summarizes the phase-matching results for all three principal planes and the off-principal-plane optimum for Type-II SHG, confirming that the XY plane is the only principal plane where phase matching is achievable and that the off-axis orientation yields a superior residual mismatch.

plane	Phase-matching angle	$n_{slow}(\omega)$	$n_{fast}(\omega)$	$n_{fast}(2\omega)$	Δn
XY	φ=51.3514, θ=90	1.605053	1.574956	1.589996	9.0642×10^{-6}
XZ	φ=0, θ=0	1.590323	1.565050	1.578883	1.1967×10^{-3}
YZ	φ=90, θ=11.4414	1.565050	1.565048	1.578883	1.3834×10^{-2}
Off-axis	φ=64.4147°, θ=39.4314°	1.595701	1.567557	1.581629	6.1457×10^{-8}

3.5 Walk-off Analysis

In birefringent phase-matching crystals, the walk-off effect arises because the Poynting vector of an eigenmode propagating in a birefringent crystal is not parallel to the wave vector The walk-off angle ρ, defined as the angle between the Poynting vector **S** (energy flow direction) and the wave vector **k** (phase propagation direction), arises because in an anisotropic medium the Poynting vector is perpendicular to the index ellipsoid surface, whereas the wave vector is directed along the wave normal, two directions that generally do not coincide except along the principal crystallographic axes. This phenomenon is a critical constraint in nonlinear optics, as it limits the effective interaction length and the beam quality of the generated light.

For SHG, walk off leads to spatial separation between the fundamental and harmonic beams

reducing their overlap and limiting the effective nonlinear interaction length thereby lowering the conversion efficiency [9]. Energy propagates along with the group velocity, which is given by the relation[1].

$$v_g=\frac{\partial\omega}{\partial k} \quad (11)$$

The walk-off angle ρ represents the angle between the directions of the group velocity and the wave vector for cases of weak inhomogeneity, this angle can be approximated by the relation:

$$\tan\rho \approx \frac{|\nabla n|}{n} \quad (12)$$

where the refractive index depends on the direction of propagation n = n(θ, φ) and ∇ represents the angular gradient of the refractive index in terms of the propagation angles on the unit sphere. The angular gradient of the refractive index is given by the relation

$$\nabla n = \hat{\theta}\,\frac{\partial n}{\partial\theta} + \hat{\varphi}\,\frac{1}{sin\theta}\frac{\partial n}{\partial\varphi}$$

$$\nabla n| = \sqrt{\left(\frac{\partial n}{\partial\theta}\right)^2 + \frac{1}{\sin^2\theta}\left(\frac{\partial n}{\partial\varphi}\right)^2}$$

(13)

So, the general expression for the ray walk off angle of a wave propagation inside a biaxial crystal in the direction (θ, φ) is [1]

$$\rho = \tan^{-1}\left(\frac{1}{n}\sqrt{\left(\frac{\partial n}{\partial\theta}\right)^2 + 1/\sin^2\theta\,\left(\frac{\partial n}{\partial\varphi}\right)^2}\right)$$

(14)

Where $\frac{\partial n}{\partial\theta}\ and\ \frac{\partial n}{\partial\varphi}$ are obtained by differentiating (Eq.7) with respect to θ and φ, respectively.

3.5.1 Walk-off angle as a function of wavelength for type I SHG

The spectral dependence of the walk-off angle in the LBO in relation to type I SHG has been studied within the three principal planes as follows:

a) Walk-off in XY-Plane (θ=90°)

Left side of Fig.7 shows walk off angle in the XY plane. LBO exhibits a specific spectral window of low walk-off, from 0.2μm to 0.6μm, the angle remains nearly zero. In this spectral region, the phase-matching angles approach the principal crystallographic axes, where the walk-off angle naturally tends toward zero, a behavior analogous to the low-walk-off advantage of non-critical phase matching. Then near 0.6μm, ρ increases sharply, reaching a maximum of approximately 0.95° near 0.8 μm. This peak corresponds to the region of strongest birefringence, where the angular sensitivity of the phase-matching condition (critical phase matching) is highest and the deviation between energy flow and phase propagation directions is greatest. This indicates a transition into Critical Phase Matching (CPM), where the efficiency becomes highly sensitive to the alignment and beam divergence, birefringence is strongest and maximum deviation between energy and phase velocity. At longer wavelengths, ρ decreases gradually due to the reduction in dispersion and birefringence at infrared wavelengths.

b) Walk-off in XZ-Plane (φ=0°)

The right panel of Fig. 7 shows the spectral dependence of the walk-off angle in the XZ plane. Walk-off, ρ, remains negligibly small below 0.66 μm, then it increases steadily into the near-infrared, reaching approximately 1.38° at 1.1μm. At this level of walk-off, spatial separation between the interacting beams becomes significant, leading to beam astigmatism and a degraded second-harmonic beam profile that reduces the effective nonlinear interaction length

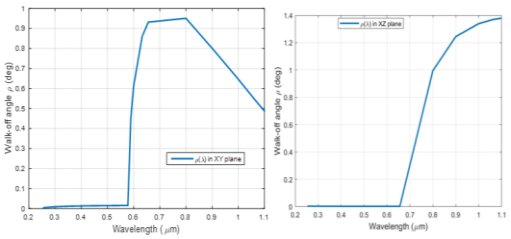

Fig. 7: the Spectral Dependence of Walk-off Angle (rho) for Type I SHG Phase Matching in LBO. Left : XY plane, right: XZ plane

c) Walk-off in the YZ-Plane (φ=90º)

For the propagation in the YZ plane, **k** = (0, sinθ , cosθ). The two polarization eigenmodes are: (1) the X-polarized mode, carrying the pure principal index n_x, which has no angular dependence in this plane ($\partial n_x/\partial\theta = 0$), giving identically zero walk-off and (2) the in-plane mode, mixing n_y and n_z, which carries a finite but small walk-off owing to the modest birefringence $|n_z - n_y| \approx 0.015$ in the LBO.

Despite this low walk-off, Type-I phase matching is not achievable in the YZ plane for the SHG at 1.064 μm. The maximum available birefringence is insufficient to compensate the dispersion between ω and 2ω, and no angle θ satisfies $n_{fast}(2\omega) = n_{slow}(\omega)$. This follows from the fact that the optical axes of LBO lie entirely within the XZ plane and do not intersect the YZ plane. The YZ plane is therefore unsuitable for SHG regardless of its favorable walk-off.

3.5.2 Walk-off Surface for Type-I SHG for λ=1064

Fig. 8 shows the 3D walk-off surface ρ(θ, φ) for LBO at λ = 1.064 μm. The walk-off angle peaks near θ ≈ 45–50° at lower ϕ values, reaching approximately 1.38°, consistent with literature values [1]. These are the propagation directions where the energy flow deviates most from the wave vector due to maximum birefringence anisotropy. Near θ = 0° and θ = 90°, the walk-off drops to near zero. This behavior perfectly correlates with the principal plane propagation geometry discussed in section 3.3.1, where one eigenmode carries a pure principal index because propagation approaches the principal crystallographic axes, where one eigenmode carries a pure principal index with no angular gradient, forcing the Poynting vector to align with the wave vector.

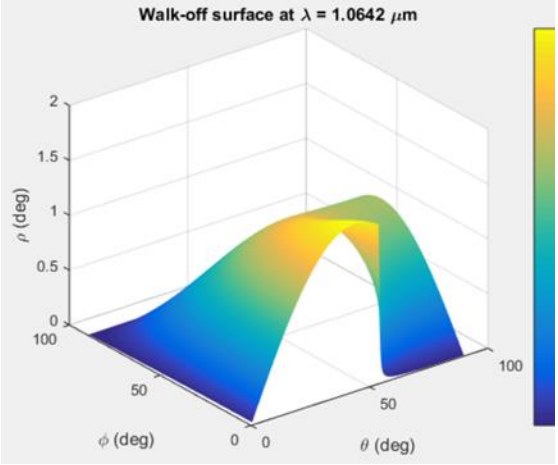

Fig.8: 3D surface of the walk-off angle (ρ) for biaxial crystal LBO at (λ = 1.0642μm), plotted as a function of the propagation angles (θand φ).

3.6 Spectral Tuning of OPO in LBO

Fig.9 illustrates the angular tuning characteristics for an LBO based Optical Parametric Oscillator (OPO, pumped at λ_p=532 nm, for both Type I and Type II interactions.

3.6.1 Type I OPO Tuning (XY and XZ Planes)

In Type-I phase matching, the signal and idler share the same polarization (fast axis, XY plane), orthogonal to the Z-polarized pump. In the XY plane, φ tunes from ~7.5° to ~10.7°, producing broad wavelength coverage with small angular shifts due to the strong azimuthal birefringence tunability of this plane. In the XZ plane, a very narrow angular range (~31.7° to ~32°) yields a large spectral shift, reflecting the stronger angular sensitivity of birefringence in this plane. In both planes, signal and idler converge at the degenerate point λs = λi = 2λp = 1064 nm.3.6.2 Type II OPO Tuning (XY Plane θ=90º).

The narrow angular tuning range required in the XZ plane (~31.7° to ~32°) for a large spectral shift reflects the steeper angular gradient of birefringence in that plane compared to the XY plane, where a broader angular sweep (~7.5° to ~10.7°) is needed for equivalent wavelength coverage. This difference has practical implications: XZ-plane OPO devices are more sensitive to crystal angular tolerances, while XY-plane devices tolerate larger beam divergence.

3.6.2 Type II OPO Tuning (XY Plane θ=90º)

In Type-II phase matching (fig.9), signal and idler carry orthogonal polarizations. As φ increases from 0° to ~60°, the signal sweeps from the near-IR up to ~2.5 μm while the idler descends. At φ ≈ 30°, signal and idler reach equal wavelengths (1064 nm), corresponding to the degenerate point, not a polarization crossing, since the two beams remain distinguishable by their orthogonal polarization states throughout.

The extension of the Type-II signal to 2.5 μm is a direct consequence of the additional degree of freedom provided by the orthogonal polarization constraint, which allows a larger index difference between signal and idler to be sustained across a wider wavelength range. This mid-infrared coverage makes Type-II XY-plane operation particularly attractive for spectroscopic applications in the 2–3 μm atmospheric window. It should be noted that the

present OPO analysis is confined to the phase-matching geometry and does not include gain bandwidth calculations threshold pump intensity estimates or cavity design considerations A complete OPO design would additionally require the effective nonlinear coefficient d_{eff}, the signal, idler group velocity dispersion and the round trip cavity loss, these aspects are identified as important directions for future work.

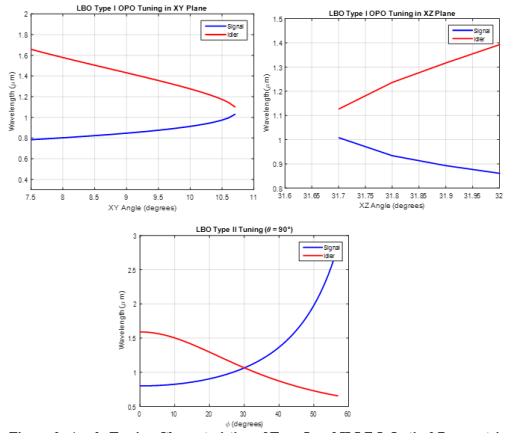

Figure 9: Angle-Tuning Characteristics of Type I and II LBO Optical Parametric Oscillators (OPO) in XY and XZ Planes for $\lambda p = 532nm$.

3.7 Numerical Validation

The principal-planes phase-matching angles computed in this work are validated against the established experimental and theoretical literature values for LBO For Type-I SHG at 1.064μm, the XY Plane cut angle of $\varphi = 16.13^{o}$ is consistent with the widely cited value of 11.4^{o} - 16^{o} reported in [1, 3, 10] depending on the Sellmeier parameterization employed. The XZ-plane angle of $\theta = 30.99^{o}$ agrees with the range $\theta = 29^{o}$ - 32^{o} tabulated in [1, 2] for Type-II SHG the XY-plane cut of $\varphi = 51.35^{o}$ at $\theta = 90^{o}$ is consistent with values reported in [10, 11].

The principal refractive indices at $\lambda = 1.064\mu m$ (Table 2) agree to within 0.2% with the values listed in the standard reference [1]. The walk-off peak of ~ 0.95^{o} in the XY plane and ~ 1.38^{o} in the XZ plane at 1.064μm are in excellent agreement with the standard values 0.95^{o} and 1.28^{o} decumented in reference [1].

While direct experimental measurements for off-principal planes phase maching angles are currently unavailable in the literature, the reliability of these theoretical predictions is quantitatively supported by the model's internal consistency [7,8]. The two dimentional phase maching surface accurately reproduces the well- established principal plane values at its cross-sections: the $\theta=90^{o}$ cross section matches the XY plane minimum, and the $\phi=0^{o}$ cross section matches the XZ plane minimum [9 and 10] furthermore the model identifies global off- axis optima with extremily low residual mismatches $\Delta n=1.02*10^{-7}$ for type I and $\Delta n=6.15*10^{-8}$ for type II, which represent a significant improvement in phase matching precision compared to principal plane results.

While this study establishes the geometric foundation of phase matching, several critical parameters for practical device design remain for future investigation. Specifically, the effective nonlinear coefficient (d_{eff}) and the SHG conversion efficiency (η) were not computed in this work. Additionally, since the current model

operates at room temperature, future work should incorporate thermal effects, such as thermos-optic dispersion and linear two photon absorption, which are indispensable for the design of high average- power LBO devices [3].

4. Conclusions

A comprehensive numerical model has been developed for the angular and spectral phase-matching analysis of Type-I and Type-II nonlinear interactions in the LBO crystals, based on solving the Fresnel equation using modified Sellmeier coefficients. The model simultaneously addresses the spectral birefringence characterization, critical phase-matching optimization, walk-off quantification, and OPO parametric tuning within a single self-consistent framework.

For Type-I SHG at 1.064 μm, phase matching is achieved in the XY plane at $\varphi = 16.13°$ ($\Delta n = 2.85\times10^{-6}$) and in the XZ plane at $\theta = 30.99°$ ($\Delta n = 2.34\times10^{-5}$). A full two-dimensional angular scan identifies a global off-principal-plane optimum at $\theta = 67.42°$,$\varphi = 25.59°$, yielding a near-perfect phase mismatch of $\Delta n = 1.02\times10^{-7}$. For Type-II SHG, phase matching is found in the XY plane at $\varphi= 51.35°$ ($\Delta n = 9.06\times10^{-6}$), with an off-axis optimum at $\theta = 39.43°$, $\varphi = 64.41°$ ($\Delta n = 6.15\times10^{-8}$). Phase matching is not achievable in the YZ plane for either interaction type, as the available birefringence $|n_z - n_y|$ is insufficient to compensate the dispersion at this fundamental wavelength.

To the authors' knowledge, no published experimental measurements exist for off-principal-plane cut angles, and these results represent original theoretical predictions.

Walk-off analysis shows that the XY plane offers a low-walk-off spectral window below 0.6 μm, making it favorable for high-efficiency SHG in the UV-visible range. In the XZ plane, walk-off increases steadily into the near-infrared, reaching ~1.38° at 1.1 μm, imposing a practical limit on the usable crystal length. The 3D walk- off surface confirms that maximum walk-off occurs near $\theta = 45–50°$ at low φ values, and drops to near zero along the principal crystallographic axes.

For the OPO pumped at 532 nm, Type-I tuning in the XY and XZ planes provides coverage toward for the degenerate point at 1064 nm, while Type-II tuning in the XY plane extends the signal wavelength up to 2.5 μm through azimuthal rotation, demonstrating the superior mid-infrared coverage that is achievable with Type-II interaction in the LBO.

These concluding points provide a practical and systematic framework for the design and optimization of the LBO-based nonlinear optical devices, and establish clear guidelines for cut-angle selection balancing phase-matching quality, walk-off minimization, and spectral tuning range.

The effective nonlinear coefficient d_{eff} and the SHG conversion efficiency η for the principal planes and off

planes, are important parameters for practical device design that are not computed in the present study, and recommended to be studied in the next work.

References

[1] V. G. Dmitriev, G. G. Gurzadyan, and D. N. Nikogosyan, *Handbook of Nonlinear Optical Crystals*, vol. 64, Berlin: Springer, 2013.

[2] D. N. Nikogosyan, *Nonlinear Optical Crystals: A Complete Survey*, New York: Springer, 2005.

[3] C. Chen, Y. Wu, A. Jiang, B. Wu, G. You, R. Li, and S. Lin, "New nonlinear-optical crystal: LiB_3O_5," *Journal of the Optical Society of America B*, vol. 6, no. 4, pp. 616–621, 1989.

[4] T. J. Johnston Jr. and J. P. Pique, "Broadly tunable, single-frequency optical parametric oscillators," *Applied Optics*, vol. 32, no. 30, pp. 6605–6610, 1993.

[5] F. Laurell, "Stable blue second-harmonic generation in KTP and LBO with moderate power," *Optics Letters*, vol. 20, no. 7, pp. 704–706, 1995.

[6] M. Born and E. Wolf, *Principles of Optics: Electromagnetic Theory of Propagation, Interference and Diffraction of Light*, 7th ed., Cambridge: Cambridge University Press, 1999.

[7] B. D. Guenther and D. Steel, *Encyclopedia of Modern Optics*, 2nd ed., Amsterdam: Academic Press, 2018.

[8] R. W. Boyd, *Nonlinear Optics*, 3rd ed., Burlington: Academic Press, 2008.

[9] K. Kato, "Parametric oscillation at 3.2 μm in KTP pumped at 1.064 μm," *IEEE Journal of Quantum Electronics*, vol. 27, no. 5, pp. 1137–1140, 1991; and specifically for LBO Sellmeier: K. Kato, "Second-harmonic generation to 2048 Å in β-BaB_2O_4," *IEEE Journal of Quantum Electronics*, vol. 22, no. 7, pp. 1013–1014, 1986. *(Sellmeier equation determinations for nonlinear crystals including LBO)*

[10] O. K. Swarupa, R. K. Biswal, P. K. Das, and S. K. Das, "Angular birefringence phase matching behaviour of Lithium Triborate (LBO) crystal for second harmonic generation in broad wavelength range," *Materials Today: Proceedings*, vol. 62, pp. 6221–6226, 2022.

[11] T. Schröder, K.-J. Boller, A. Fix, and R. Wallenstein, "Spectral properties and numerical modelling of a critically phase-matched nanosecond LiB_3O_5 optical parametric oscillator," *Applied Physics B*, vol. 58, pp. 425–438, 1994.

[12] H. Liu, F. Wang, L. Sun, T. Zheng, and F. Wang, "Laser damage properties of LiB_3O_5 crystal surface under UV laser irradiation," *Optics Express*, vol. 31, pp. 30184–30193, 2023.

[13] R. Majid Hilal and S. Y. Hasan, " Optical Dispersion and Velocity Characteristics of Lithium Triborate (LBO)" Tmrees26 (International Conference on Technologies and Materials for Renewable Energy, Environment and Sustainability)(2026).